The Electromagnetic Form Factors of Σ and $\Sigma^0 \to \Lambda$ Transition in the Timelike Region

Cheng Chen(陈诚)[1,2], Bing Yan(闫冰)[3], Bing-Wei Long(龙炳蔚)[3,4], and Ju-Jun Xie(谢聚军)[1,2,4*]

[1]*State Key Laboratory of Heavy Ion Science and Technology, Institute of Modern Physics, Chinese Academy of Sciences, Lanzhou 730000, China*
[2]*School of Nuclear Sciences and Technology, University of Chinese Academy of Sciences, Beijing 101408, China*
[3]*College of Physics, Sichuan University, Chengdu 610065, China*
[4]*Southern Center for Nuclear-Science Theory (SCNT), Institute of Modern Physics, Chinese Academy of Sciences, Huizhou 516000, China*

(Received 9 July 2025; accepted manuscript online 16 October 2025)

We investigate the $e^+e^- \to \Sigma\bar{\Sigma}$ and $e^+e^- \to \Lambda\bar{\Sigma}^0$ reactions within the extended vector meson dominance model. In addition to the ground state mesons ρ and ω, we consider the contributions of the excited states $\rho(3D)$, $\omega(3D)$, $\phi(3D)$, and $\rho(2850)$. It is found that the current experimental data on the Σ electromagnetic form factors in timelike region can be well reproduced. The $\phi(3D)$ resonance is essential to the near threshold enhancement of the cross-section for the $e^+e^- \to \Sigma\bar{\Sigma}$ reaction. Furthermore, in the $e^+e^- \to \Lambda\bar{\Sigma}^0$ reaction, the $\rho(3D)$ is important to get a good fit for the experimental results.

DOI: 10.1088/0256-307X/42/12/120201 CSTR: 32039.14.0256-307X.42.12.120201

1. Introduction. The electromagnetic form factors (EMFFs) of baryons encode crucial information about their electromagnetic structure,[1–3] which depends on the squared of four-momentum transfer, q^2, of the interacted virtual photon. Hence, investigating the EMFFs of baryons is essential for gaining deeper insight into their fundamental structure. The region where $q^2 < 0$ is referred to as the spacelike region, while $q^2 > 0$ is known as the timelike region. In the spacelike region, EMFFs are real and relate to the charge and magnetic distribution of baryons. In contrast, EMFFs in the timelike region are generally complex. Interestingly, an analytical study revealed that EMFFs in the timelike region tend to become real at large four-momentum transfer squared.[4] Furthermore, reference [5] proposed that, in the timelike region, these EMFFs are connected to the time evolution of baryons' electromagnetic distributions. On the experimental side, measuring the EMFFs of unstable baryons, such as hyperon Σ, Λ, and Ξ, through electron-baryon scattering in the spacelike region is challenging due to their short lifetimes. Consequently, it is more practical to study baryon EMFFs in the timelike region using electron-positron annihilation reactions. Significant experimental progress has been made in measuring hyperon EMFFs in the timelike region.[6–17] Recent advancements in experimental techniques and increased statistics have considerably reduced measurement uncertainties. Experimentally, near the production threshold, enhancements in the total cross-sections were observed in the processes $e^+e^- \to N\bar{N}, \Lambda\bar{\Lambda}$ and $\Lambda_c^+\bar{\Lambda}_c^-$.[18] Additionally, spin polarization distributions of final-state baryons have been obtained in reactions such as $e^+e^- \to \Lambda\bar{\Lambda}$,[19–22] $e^+e^- \to \Sigma\bar{\Sigma}$,[23–26] and $e^+e^- \to \Xi\bar{\Xi}$.[27–30] These rich experimental data have sparked extensive theoretical interest in studying EMFFs of the hyperons and related topics.[31–45]

For the $e^+e^- \to \Sigma\bar{\Sigma}$ process, experimental measurements from the BESIII Collaboration reveal that the total cross-section ratios for the reactions $e^+e^- \to \Sigma^+\bar{\Sigma}^-$, $\Sigma^0\bar{\Sigma}^0$, and $\Sigma^-\bar{\Sigma}^+$ are $9.7\pm1.3 : 3.3\pm0.7 : 1$ over a center-of-mass energy range of 2.3864 GeV to 3.02 GeV.[46–48] These ratios deviate significantly from predictions made by various theoretical models.[49–51] The discrepancy has drawn considerable attention, prompting theoretical investigations from different perspectives. The vector meson dominance (VMD) model, a well-established framework for studying nucleon EMFFs in both space and timelike regions,[52–55] has also been extended to the hyperon sector.[34–38] In this model, the virtual photon couples to baryons via intermediate vector mesons. In our earlier work, we applied the VMD model to the $e^+e^- \to \Sigma\bar{\Sigma}$ process, considering only the ground states of vector mesons. This approach successfully reproduced the observed cross-section ratios.[37] However, the new BESIII measurements for the reaction $e^+e^- \to \Sigma^+\bar{\Sigma}^-$ show higher central values compared to those of previous measurements.[15,46] Additionally, the findings suggest the potential existence of a new resonance at $\sqrt{s} = 2.5$ GeV.[15] These findings indicate that considering only the ground of vector mesons is insufficient to fully account for current experimental data; therefore, contributions from excited vector states should be incorporated into the model.

*Corresponding author. Email: xiejujun@impcas.ac.cn
© 2025 Chinese Physical Society and IOP Publishing Ltd. All rights, including for text and data mining, AI training, and similar technologies, are reserved.

The total cross-section of the $e^+e^- \to \Lambda\bar{\Sigma}^0$ reaction were measured for the first time by BaBar Collaboration,[6] and it was recently re-measured by the BESIII Collaboration with improved precision.[16] The two groups of experimental data are similar, except for the one closed to the reaction threshold. The BESIII Collaboration obtained a total cross-section $72.9 \pm 12.6 \pm 5.4$ pb with a statistical significance greater than 5 standard deviations at a center-of-mass energy just about 1 MeV above the threshold. The fit results given at 2.386 GeV seem to exceed the upper limit of 75 pb set by the DM2 Collaboration.[56] In Ref. [33], the authors used various $\Lambda\bar{\Sigma}^0$ potential forms from Ref. [57] as final state interactions to reproduce the near-threshold $e^+e^- \to \Lambda\bar{\Sigma}^0$ cross-section measured by BaBar Collaboration. Their results showed a sudden increase in the cross-section near the threshold, followed by a plateau extending over 100 MeV. However, this behavior is inconsistent with the latest experimental data from BESIII Collaboration,[16] suggesting that additional mechanisms must be taken into account.

For excited states of vector mesons, numerous experimental results are documented in the Particle Data Group (PDG).[58] However, experimental discoveries for light vector mesons with masses above 2 GeV remain limited. As a result, most studies on highly excited vector mesons rely on theoretical approaches.[59–69] In Ref. [60], the excited states of ρ and ω mesons were explored within the 2.0–2.4 GeV mass range. The $\rho(3D)$ and $\omega(3D)$ states were identified with masses of 2.283 GeV and widths of 158 MeV and 94 MeV, respectively; both lie close to the $\Sigma\bar{\Sigma}$ threshold. In Ref. [61], the mass and decay properties of ρ, ω, and ϕ meson excited states in the 2.4–3.0 GeV range were investigated using the modified Godfrey–Isgur model which identified six excited states for each meson within this interval. Additionally, the studies in Ref. [70] expanded on the decay properties of highly excited ρ states by considering additional decay channels beyond those in Ref. [61]. Furthermore, the decay of ϕ excited states into $\Lambda\bar{\Lambda}$, $\Sigma\bar{\Sigma}$, and $\Xi\bar{\Xi}$ was also examined using the hadronic-loop mechanism.[67] It was found that the $\phi(3D)$ state at 2.5 GeV decays into $\Sigma\bar{\Sigma}$ with a relatively significant branching ratio suggesting its potential importance in the $e^+e^- \to \Sigma\bar{\Sigma}$ reaction.

Based on these theoretical predictions and the vector mesons listed in the PDG,[58] we include the $\rho(3D)$, $\omega(3D)$, $\phi(3D)$, and $\rho(2850)$ states for studying the $e^+e^- \to \Sigma\bar{\Sigma}$ and $e^+e^- \to \Lambda\bar{\Sigma}^0$ reactions within the framework of the VMD model. The $\rho(2850)$ state was introduced to account for experimental data at a center-of-mass energy of 2.9 GeV, with its mass and width set to 2.850 GeV and 150 MeV, respectively. Their masses and widths are summarized in Table 1.

Table 1. The mass and width of the states used for this work. We take an averaged mass and width for ω and ϕ mesons.

State	Mass $M_{\rm R}$ (MeV)	Width $\Gamma_{\rm R}$ (MeV)	Reference
ρ	775	149.1	[58]
$\omega\phi$	900.5	6.46	[58]
$\rho(3D)$	2300	160	[60]
$\omega(3D)$	2300	100	[60]
$\phi(3D)$	2500	170	[61,67]

This article is organized as follows: in Section 2, we outline the theoretical framework for calculating the EMFFs of the Σ and Λ–$\bar{\Sigma}^0$ transition within the VMD approach. Numerical results and discussions are presented in Section 3. Finally, a brief summary and conclusions are provided in the last section.

2. Formalism. For the $e^+e^- \to \Sigma\bar{\Sigma}$ reaction, the interaction vertex of $\gamma^*\Sigma\bar{\Sigma}$ can be parameterized to two independent form factors $F_1(q^2)$ and $F_2(q^2)$, referred to as the Dirac and Pauli form factors, respectively, according to electromagnetic current conservation and CP invariance. Therefore, the matrix element of $\Sigma\bar{\Sigma}$ created by electromagnetic current from the vacuum can be expressed as $\langle\Sigma\bar{\Sigma}|J^{\rm em}_\mu|0\rangle = \bar{u}_\Sigma(p_\Sigma, s_\Sigma)\Gamma_\mu v_{\bar{\Sigma}}(p_{\bar{\Sigma}}, s_{\bar{\Sigma}})$ with $\Gamma_\mu = \gamma_\mu F_1(q^2) + {\rm i}F_2(q^2)\sigma_{\mu\nu}q^\nu/(2M_\Sigma)$, q is four-momentum of the virtual photon γ^*, and M_Σ is the mass of Σ hyperon. Then the electric $G_{\rm E}$ and magnetic form factor $G_{\rm M}$ can be obtained by combining the Pauli and Dirac form factors,

$$G_{\rm E}(q^2) = F_1(q^2) + \tau F_2(q^2), \tag{1}$$

$$G_{\rm M}(q^2) = F_1(q^2) + F_2(q^2), \tag{2}$$

with $\tau = q^2/(4M_\Sigma^2)$. Within the $G_{\rm M}$ and $G_{\rm E}$, the total cross-section of the $e^+e^- \to \Sigma\bar{\Sigma}$ reaction in the center of mass frame is obtained as

$$\sigma(e^+e^- \to \Sigma\bar{\Sigma}) = \frac{4\pi\alpha^2_{\rm em}\beta C}{3s}\left(|G_{\rm M}|^2 + \frac{1}{2\tau}|G_{\rm E}|^2\right), \tag{3}$$

where $s = q^2$ is the invariant mass squared of the e^+e^- system, $\alpha_{\rm em} = e^2/4\pi = 1/137.036$ is the electromagnetic fine structure constant, and $\beta = \sqrt{1 - 4M_\Sigma^2/s}$ is the velocity of Σ hyperon. The factor C is the S-wave Sommerfeld–Gamow factor originating from the Coulomb interaction of the final $\Sigma\bar{\Sigma}$.[71] We take $C = 1$ for $\Sigma^0\bar{\Sigma}^0$ and $C = \frac{y}{1-e^{-y}}$ for $\Sigma^+\bar{\Sigma}^-$ and $\Sigma^-\bar{\Sigma}^+$, and here $y = 2\pi\alpha_{\rm em}M_\Sigma/(\beta\sqrt{s})$. Thus, for charged Σ^+ and Σ^-, the total cross-section of their responding is non-zero at the reaction threshold. Moreover, the Coulomb interaction just affects the reaction threshold about a few MeV, and it decreases rapidly and exponentially to a constant 1.

According to the total cross-section Eq. (3), we can extract the so-called effective form factor $|G_{\rm eff}|$,

$$|G_{\rm eff}(q^2)| = \sqrt{\frac{2\tau|G_{\rm M}(q^2)|^2 + |G_{\rm M}(q^2)|^2}{1 + 2\tau}}. \tag{4}$$

Moreover, we can also obtain the differential cross-section distribution parameter α in the reaction,

$$\alpha = \frac{s|G_{\rm M}|^2 - 4M_\Sigma^2|G_{\rm E}|^2}{s|G_{\rm M}|^2 + 4M_\Sigma^2|G_{\rm E}|^2}, \tag{5}$$

which only depends on the ratio of the absolute values of EMFFs and satisfies $-1 \le \alpha \le 1$.

In the timelike region, $G_{\rm E}$ and $G_{\rm M}$ are complex, and their relative phase $\Delta\Phi$ is an observable quantity that can be extracted from the spin polarization of the final hyperons[19–27,29,30] and the spin polarization distribution along the direction $\hat{p} \times \hat{k}$ ($\hat{k}$ is the momentum direction of

electron, and $\hat{p}$ is the momentum direction of Σ hyperon in the center-of-mass frame). The relationship is given by [72]

$$P_y(\theta) = \frac{\sqrt{1-\alpha^2}\sin\theta\cos\theta}{1+\alpha\cos^2\theta}\sin\Delta\Phi, \tag{6}$$

where θ is the scattering angle between the electron and Σ hyperon. At a fixed center-of-mass energy, the maximum value of the polarization P_y occurs when $\cos^2\theta = 1/(2+\alpha)$ with $P_y{}^{\max} = \frac{1}{2}\sqrt{1-\alpha}\sin\Delta\Phi$. Further details regarding polarization observables in the timelike region are provided in the supplementary Materials (SM).

For the $e^+e^- \to \Lambda\bar{\Sigma}^0$ reaction, the matrix of the $\Lambda\bar{\Sigma}^0$ created by the electromagnetic current is given by [73]

$$\langle\Lambda\bar{\Sigma}^0|J_\mu^{\rm em}|0\rangle = \bar{u}_\Lambda(p_\Lambda,s_\Lambda)\Big[\Big(\gamma_\mu - \frac{M_\Lambda - M_{\bar{\Sigma}^0}}{q^2}q^\mu\Big)F_1(q^2) + {\rm i}\frac{F_2(q^2)}{M_{\bar{\Sigma}^0}+M_\Lambda}\sigma_{\mu\nu}q^\nu\Big]v_{\bar{\Sigma}^0}(p_{\bar{\Sigma}^0},s_{\bar{\Sigma}^0}). \tag{7}$$

Similarly, the total cross-section of the reaction is

$$\sigma(e^+e^-\to\Lambda\bar{\Sigma}^0) = \frac{4\pi\alpha_{\rm em}^2\beta}{3s}\Big(|G_{\rm M}|^2 + \frac{1}{2\tau}|G_{\rm E}|^2\Big) \tag{8}$$

with $\tau = q^2/(M_{\Sigma^0}+M_\Lambda)^2$, and β is given by

$$\beta = \sqrt{1-\frac{2(M_{\bar{\Sigma}^0}^2+M_\Lambda^2)}{q^2}+\Big(\frac{M_{\bar{\Sigma}^0}^2-M_\Lambda^2}{q^2}\Big)^2}. \tag{9}$$

In our previous work,[37] only ground vector mesons ρ, ω, and ϕ were included in the reaction $e^+e^-\to\Sigma\bar{\Sigma}$. Here, we will also include the excited vector states around 2 GeV. Since $\rho(3D)$ and $\omega(3D)$ have the same mass, it is difficult to determine the contribution of each of $\rho(3D)$ and $\omega(3D)$ if both are included in the VMD model. Therefore to analyse the effect of $\rho(3D)$ and $\omega(3D)$, and also to reduce the parameters, we considered two scenarios in the model: in Scenario I, ρ, ω, ϕ, $\omega(3D)$, $\phi(3D)$, and $\rho(2850)$ are considered; while in Scenario II, $\omega(3D)$ is replaced by $\rho(3D)$.

For Scenario I, the Dirac and Pauli form factors F_1 and F_2 for Σ isospin triplet states in the timelike region can be parametrized as

$$F_1^{\Sigma^\pm} = g(q^2)\Big(f_1^{\Sigma^\pm} \pm \frac{\beta_\rho}{\sqrt{2}}B_\rho + \frac{\beta_{\omega\phi}}{\sqrt{3}}B_{\omega\phi} + \frac{\beta_{\omega(3D)}}{\sqrt{3}}B_{\omega(3D)} + \frac{\beta_{\phi(3D)}}{\sqrt{3}}B_{\phi(3D)} \pm \frac{\beta_{\rho(2850)}}{\sqrt{2}}B_{\rho(2850)}\Big), \tag{10}$$

$$F_2^{\Sigma^\pm} = g(q^2)\Big(f_2^{\Sigma^\pm}B_\rho + \frac{\alpha_{\omega\phi}}{\sqrt{3}}B_{\omega\phi} + \frac{\alpha_{\omega(3D)}}{\sqrt{3}}B_{\omega(3D)} + \frac{\alpha_{\phi(3D)}}{\sqrt{3}}B_{\phi(3D)} \pm \frac{\alpha_{\rho(2850)}}{\sqrt{2}}B_{\rho(2850)}\Big), \tag{11}$$

for Σ^+ and Σ^-, and

$$F_1^{\Sigma^0} = g(q^2)\Big(f_1^{\Sigma^0} + \frac{\beta_{\omega\phi}}{\sqrt{3}}B_{\omega\phi} + \frac{\beta_{\omega(3D)}}{\sqrt{3}}B_{\omega(3D)} + \frac{\beta_{\phi(3D)}}{\sqrt{3}}B_{\phi(3D)}\Big), \tag{12}$$

$$F_2^{\Sigma^0} = g(q^2)\Big(f_2^{\Sigma^0}B_{\omega\phi} + \frac{\alpha_{\omega(3D)}}{\sqrt{3}}B_{\omega(3D)} + \frac{\alpha_{\phi(3D)}}{\sqrt{3}}B_{\phi(3D)}\Big), \tag{13}$$

for Σ^0, with

$$B_{\rm R} = \frac{M_{\rm R}^2}{M_{\rm R}^2 - q^2 - {\rm i}M_{\rm R}\Gamma_{\rm R}}, \tag{14}$$

where the label R denotes these states: ρ, ω, ϕ, $\omega(3D)$, $\rho(3D)$, $\phi(3D)$, and $\rho(2850)$.

At $q^2 = 0$ and setting width $\Gamma_{\rm R} = 0$, the electric $G_{\rm E}$ and magnetic $G_{\rm M}$ should be equal to the charge and magnetic momentum of Σ hyperons, respectively, i.e., $G_{\rm E}^{\Sigma^+} = 1$ and $G_{\rm M}^{\Sigma^+} = \mu_{\Sigma^+}$, $G_{\rm E}^{\Sigma^0} = 0$ and $G_{\rm M}^{\Sigma^0} = \mu_{\Sigma^0}$, $G_{\rm E}^{\Sigma^-} = -1$ and $G_{\rm M}^{\Sigma^-} = \mu_{\Sigma^-}$, respectively, and then the coefficients $f_1^{\Sigma^+}$, $f_2^{\Sigma^+}$, $f_1^{\Sigma^0}$, $f_2^{\Sigma^0}$, $f_1^{\Sigma^-}$, and $f_2^{\Sigma^-}$ can be determined by these constrains,

$$f_1^{\Sigma^\pm} = \pm 1 - \frac{\beta_{\omega\phi}+\beta_{\omega(3D)}+\beta_{\phi(3D)}}{\sqrt{3}} \mp \frac{\beta_\rho+\beta_{\rho(2850)}}{\sqrt{2}}, \tag{15}$$

$$f_2^{\Sigma^\pm} = \mu_{\Sigma^\pm} \mp 1 - \frac{\alpha_{\omega\phi}+\alpha_{\omega(3D)}+\alpha_{\phi(3D)}}{\sqrt{3}} \mp \frac{\alpha_{\rho(2850)}}{\sqrt{2}}, \tag{16}$$

$$f_1^{\Sigma^0} = -\frac{\beta_{\omega\phi}}{\sqrt{3}} - \frac{\beta_{\omega(3D)}}{\sqrt{3}} - \frac{\beta_{\phi(3D)}}{\sqrt{3}}, \tag{17}$$

$$f_2^{\Sigma^0} = \mu_{\Sigma^0} - \frac{\alpha_{\omega(3D)}}{\sqrt{3}} - \frac{\alpha_{\phi(3D)}}{\sqrt{3}}, \tag{18}$$

for Σ^+, Σ^-, and Σ^0, respectively. Here, we take $\mu_{\Sigma^+} = 3.112$, $\mu_{\Sigma^-} = -1.479$, and $\mu_{\Sigma^0} = 2.044$ in natural unit $= \frac{e}{2M_\Sigma}$.[58] Corresponding expressions for F_1 and F_2 in Scenario II can easily be obtained by replacing $\omega(3D)$ with $\rho(3D)$.

The function $g(q^2)$ represents a phenomenological intrinsic form factor, typically expressed in the dipole form: $g(q^2) = 1/(1-\gamma q^2)^2$, where γ is a free parameter. However, $g(q^2)$ has a pole at $q^2 = 1/\gamma$. To prevent the pole from appearing in the physical region, γ must be greater than $1/(4M_\Sigma^2)$. It is worth noting that, in the space-like region, substituting $Q^2 = -q^2$ into the dipole form of $g(Q^2)$, along with the corresponding expressions for $F_1(Q^2)$ and $F_2(Q^2)$, makes it straightforward to derive their behavior for large Q^2. Specifically, for large Q^2, we have $F_1 \propto \frac{1}{Q^4}$ and $F_2 \propto \frac{1}{Q^6}$. These results are consistent with the asymptotic behavior of F_1 and F_2 predicted by perturbative quantum chromodynamics.[74–76]

For the case of $e^+e^-\to\Lambda\bar{\Sigma}^0$ reaction, since the total isospin of $\Lambda\bar{\Sigma}^0$ is 1, only vector mesons with isospin $I=1$ contribute to the process in the VMD model. Therefore, we consider two states: ρ and $\rho(3D)$. The Dirac and Pauli transition form factor $F_1^{\Lambda\bar{\Sigma}^0}$ and $F_2^{\Lambda\bar{\Sigma}^0}$ can be constructed as follows:

$$F_1^{\Lambda\bar{\Sigma}^0} = g(q^2)(f_1^{\Lambda\bar{\Sigma}^0} + \beta_\rho^{\Lambda\bar{\Sigma}^0}B_\rho + \beta_{\rho(3D)}^{\Lambda\bar{\Sigma}^0}B_{\rho(3D)}), \tag{19}$$

$$F_2^{\Lambda\bar{\Sigma}^0} = g(q^2)(f_2^{\Lambda\bar{\Sigma}^0}B_\rho + \alpha_{\rho(3D)}^{\Lambda\bar{\Sigma}^0}B_{\rho(3D)}), \tag{20}$$

with

$$f_1^{\Lambda\bar{\Sigma}^0} = -\beta_\rho^{\Lambda\bar{\Sigma}^0} - \beta_{\rho(3D)}^{\Lambda\bar{\Sigma}^0}, \quad f_2^{\Lambda\bar{\Sigma}^0} = \kappa - \alpha_{\rho(3D)}^{\Lambda\bar{\Sigma}^0}, \tag{21}$$

where $\kappa = -1.98$ [77,78] and $[\gamma, \beta_\rho^{\Lambda\bar{\Sigma}^0}, \beta_{\rho(3D)}^{\Lambda\bar{\Sigma}^0}, \alpha_{\rho(3D)}^{\Lambda\bar{\Sigma}^0}]$ are free model parameters.

3. Numerical Results.

3.1. The EMFFs of Σ Hyperon. We perform a χ^2-fit to the experimental data of $e^+e^-\to\Sigma\bar{\Sigma}$ reactions, including the total cross-section, the $|G_{\rm E}/G_{\rm M}|$ ratio, and the relative

Table 2. Fitted parameters in this work.

Scenario I	$\gamma(\text{GeV}^{-2})$	β_ρ	$\beta_{\omega\phi}$	$\alpha_{\omega\phi}$	$\beta_{\omega(3D)}$
	0.4217	0.9354	−0.3363	−2.8767	0.6881
	$\alpha_{\omega(3D)}$	$\beta_{\phi(3D)}$	$\alpha_{\phi(3D)}$	$\beta_{\rho(2850)}$	$\alpha_{\rho(2850)}$
	−0.7078	−0.4998	0.4856	−0.0265	0.0278
Scenario II	$\gamma(\text{GeV}^{-2})$	β_ρ	$\beta_{\omega\phi}$	$\alpha_{\omega\phi}$	$\beta_{\rho(3D)}$
	0.4662	1.4189	−0.4264	7.9466	0.0645
	$\alpha_{\rho(3D)}$	$\beta_{\phi(3D)}$	$\alpha_{\phi(3D)}$	$\beta_{\rho(2850)}$	$\alpha_{\rho(2850)}$
	−0.0968	0.3754	−0.3608	0.0537	−0.050

phase $\Delta\Phi$. There are 43 data points in total for cross-section from BESIII,[11,15,46] Belle,[13] and BaBar;[6] 6 data points of $|G_E/G_M|$ from BESIII;[24,46] and 4 data points of $\Delta\Phi$ from BESIII.[24] There are a total of 10 free parameters. The fitted parameters for both cases of Scenario I and Scenario II are presented in Table 2, and the obatined χ^2/d.o.f. are 0.9 and 1.1, respectively.

In Fig. 1, we compare our theoretical results with experimental data for the reaction $e^+e^- \to \Sigma^+\bar{\Sigma}^-$. It can be seen that by introducing these vector meson resonance states, we obtain a good description of the total cross-section as shown in Fig. 1(a), the ratio $|G_E/G_M|$ in Fig. 1(b), and the relative phase $\Delta\Phi$ in Fig. 1(c). Both Scenario I and Scenario II can describe the current experimental data. In the VMD model, considering the two mesons near the reaction threshold, in Fig. 1(a) the blue solid line and the orange one show a significant enhancement around the center-of-mass energy $\sqrt{s} = 2.5$ GeV compared to the gray line, which only includes the ground states ρ, ω, and ϕ. Notably, the blue line aligns well with the latest data from BESIII Collaboration in this region. This enhancement can be naturally attributed to contributions from $\omega(3D)/\rho(3D)$ and $\phi(3D)$. Moreover, we determined the ratio $|G_E/G_M|$ and compared it with the experimental data as illustrated in Fig. 1(b). One can clearly see that both cases of the blue and orange lines exhibit the same decreasing oscillatory pattern. This behavior is strikingly similar to the $e^+e^- \to \Lambda_c^+\bar{\Lambda}_c^-$ reaction reported by BESIII,[79] and the interpretation of the $|G_E/G_M|$ oscillations of Λ_c^+ is given by the charmonium-like vector mesons near the threshold of $\Lambda_c^+\bar{\Lambda}_c^-$,[80] which here originates from $\omega(3D)/\rho(3D)$, $\phi(3D)$, and $\rho(2850)$. Remarkably, the blue line agrees more closely with the experimental data near the threshold compared to the orange line, suggesting that the vector particles with isospin 0 may play a dominant role in the $e^+e^- \to \Sigma^+\bar{\Sigma}^-$ process.

In the timelike region, the Breit–Wigner form used in Eq. (14) will lead to a nontrivial phase to the F_1 and F_2 as well as G_E and G_M. Subsequently, we have calculated the relative phase between G_E and G_M depicted in Fig. 1(c), and the data comes from the BESIII collaboration. The data at the threshold provided by the BESIII gives two possible results.[24] Our theoretical results align well with experimental data within the margin of error. Interestingly, the phase observed at 2.9 GeV primarily stems from the interference of the $\rho(2850)$ state with other terms, which would diminish to zero without this state. The mass of this state is very close to the theoretically predicted $\rho(5D)$ or $\rho(6D)$, yet the width provided by theory

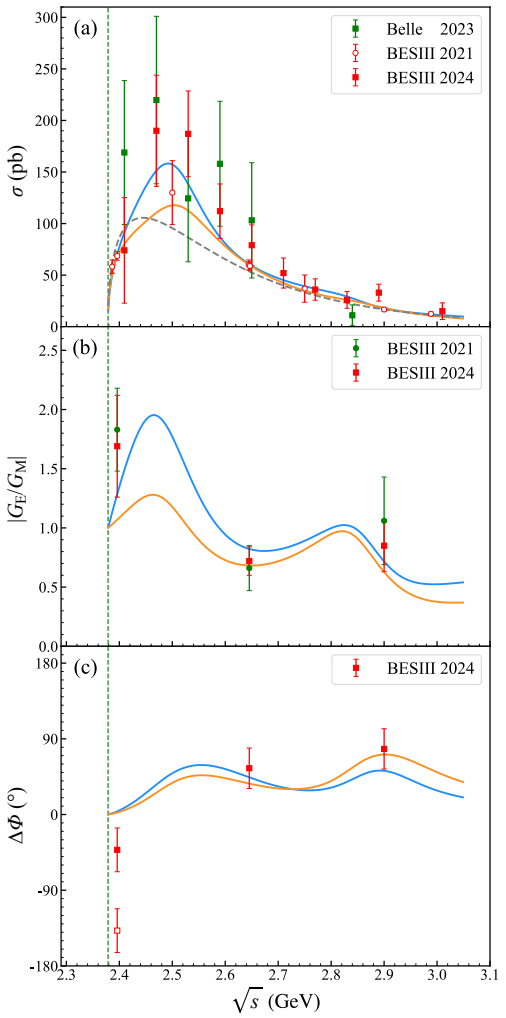

Fig. 1. The obtained total cross-sections, ratio $|G_E/G_M|$ and relative phase $\Delta\Phi$ of Σ^+ are compared with the experimental data. The blue solid line stands for Scenario I, and the orange one for Scenario II, while the gray dashed line represents our previous work.[37] The experimental data are taken from: BESIII 2021,[46] Belle 2023,[23] and BESIII 2024.[15,24] For the relative phase $\Delta\Phi$, the red square hollow represents the second solution given by BESIII.[24]

is approximately 30–50 MeV.[67,70] To match the experimental data, we adopted a relatively large width for the $\rho(2850)$; however, this width significantly exceeds the ranges predicted by theory. Additionally, references [67,70] highlight the presence of several excited ρ states in the 2.4–3.0 GeV energy range, which could collectively influence this reaction process. Incorporating these particles into the VMD framework poses challenges, as their parameters cannot be well-constrained due to insufficient data. Nonetheless, further theoretical and experimental efforts are necessary to gain a deeper understanding of these highly excited vector states.

With the obtained $|G_E/G_M|$, we also calculated the angular distribution parameter α of Σ^+ in the $e^+e^- \to \Sigma^+\bar{\Sigma}^-$ reaction, which is shown in solid lines in Fig. 2(a). In addition, with the obtained relative phase, the spin polarization of Σ^+ in the timelike region can be estimated with Eq. (6). In Fig. 2(b), we present the

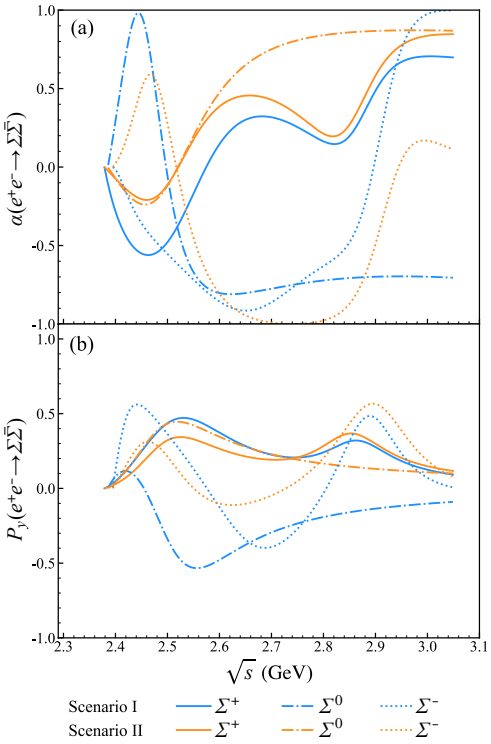

Fig. 2. The angular distribution parameter α and polarization P_y for the $e^+e^-\to\Sigma\bar{\Sigma}$ reaction.

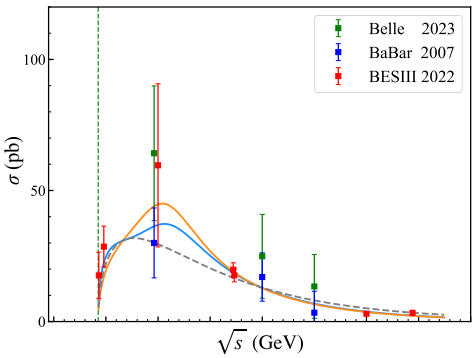

Fig. 3. The obtained total cross-sections of Σ^0 are compared with the experimental data. The blue solid line stands for the Scenario I, and orange for Scenario II, while the gray dashed line represents our previous work.[37] The experimental data are taken from Belle[13], BarBar,[6] and BESIII.[11]

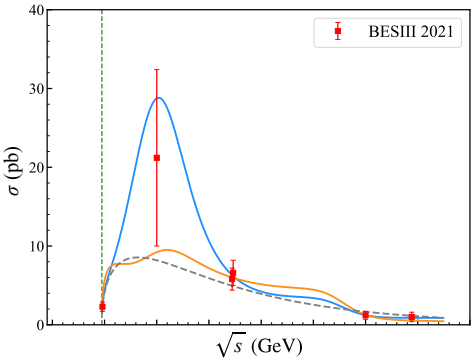

Fig. 4. The obtained total cross-sections of Σ^- are compared with the experimental data. The blue solid line stands for the Scenario I, and orange for Scenario II, while the gray dashed line represents the results of Ref. [37]. The experimental data are taken from Ref. [46].

polarization observable P_y as a function of $\sqrt{s}$ at a fixed scattering angle $\theta = 45°$. One can see that the shape of P_y will be similar to that of $\Delta\Phi$, as shown in Fig. 1(c), since P_y is proportional to $\sin\Delta\Phi$. Besides, in both cases, the polarization peak appears almost at the resonances $\phi(3D)$ and $\rho(2850)$, especially near the energy region $\sqrt{s} = 2.5$ GeV.

For the processes $e^+e^-\to\Sigma^0\bar{\Sigma}^0$ and $e^+e^-\to\Sigma^-\bar{\Sigma}^+$, the theoretical results are illustrated in Figs. 3 and 4, respectively. The blue solid line represents Scenario I, while the orange line denotes Scenario II. Currently, only experimental data on their total cross-section are available. As shown in Fig. 3, the cross-section of Σ^0 exhibits a notable enhancement around 2.5 GeV. A comparable enhancement is also seen for Σ^-, especially for Scenario I (the blue solid line), as depicted in Fig. 4. This enhancement at 2.5 GeV is attributed to the combined contributions of subthreshold $\rho(3D)$, $\omega(3D)$, and $\phi(3D)$ states for the same reason as in the reaction $e^+e^-\to\Sigma^+\bar{\Sigma}^-$. Again, we emphasize that these three vector mesons near the threshold are important to the cross-section enhancement in the reaction $e^+e^-\to\Sigma\bar{\Sigma}$. Additionally, it is feasible to consider both isospins near 2.3 GeV, just below the $\Sigma\bar{\Sigma}$ threshold. Furthermore, reference [67] predicts that the branching ratios for the decay of $\phi(3D)$ to $\Sigma\bar{\Sigma}$ are larger than those of higher excited ρ mesons predicted by the MGI model,[70] which further supports our findings.

Theoretical calculations for the ratio $|G_E/G_M|$ and relative phase $\Delta\Phi$ of Σ^0 and Σ^- are presented. As shown in Fig. 5, these two quantities for Σ^0 and Σ^- differ significantly between the two parameterizations (Scenario I and Scenario II), highlighting their sensitivity to the isospin of the vector meson excited states, specifically $\rho(3D)$ and $\omega(3D)$. The large discrepancies between the two parameterizations for Σ^0 and Σ^- can be primarily attributed to isospin decomposition effects. The same parameter set was used to describe the EMFFs of the Σ triplet states, with contributions from isospin $I = 0$ and $I = 1$ constrained by the VMD framework. For Σ^0, the $I = 1$ component does not contribute, while for Σ^-, the $I = 1$ component introduces an additional negative sign relative to the $I = 0$ component. Although substantial experimental data on cross-sections for $e^+e^-\to\Sigma\bar{\Sigma}$ processes are available, data on the ratios $|G_E/G_M|$ and relative phases $\Delta\Phi$ remain limited. This lack of data imposes relatively weak constraints on the isospin properties of vector mesons near subthreshold region. Future experimental and theoretical investigations are crucial to clarify the individual contributions of these vectors.

For Σ^0, in Fig. 5(a), the blue dash-dot curve decreases and then rises as the center-of-mass energy increases, whereas the orange dash-dot curve shows the opposite behavior, rising first and then falling. Beyond 2.7 GeV, both dash-dot curves flatten out because there is no contribution from $\rho(2850)$ in the $e^+e^-\to\Sigma^0\bar{\Sigma}^0$ process. While for Σ^-, one can see that the orange dotted line exhibits a pronounced peak in the 2.7–2.8 GeV range, indicating that the angular distribution parameter approaches -1 in this region.

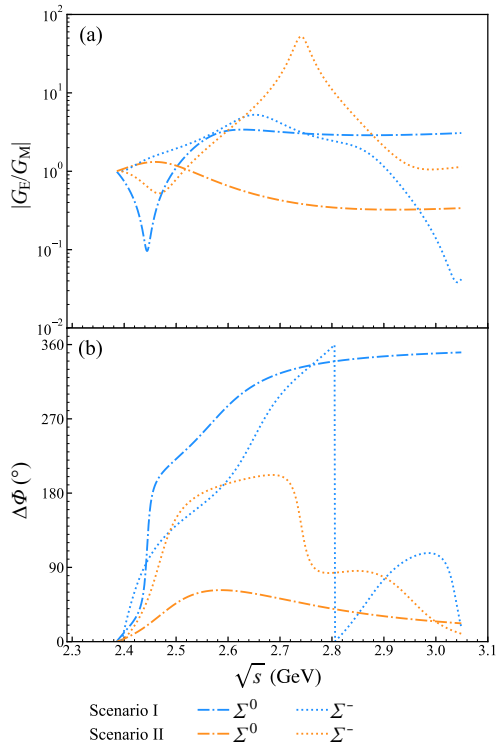

Fig. 5. The prediction for the ratio $|G_E/G_M|$ and relative phase $\Delta\Phi$ of Σ^0 and Σ^-.

As well, we get the results of α and P_y for Σ^0 and Σ^-, as displayed in Fig. 2. It can be seen that the differential cross-section for Scenario I and Scenario II exhibits different angular distributions. Therefore, measuring the differential cross-section of the reactions $e^+e^- \to \Sigma^0\bar{\Sigma}^0$ and $e^+e^- \to \Sigma^-\bar{\Sigma}^+$ is very useful for determining the different parameterizations. Note that in Fig. 5(b), the phase $\Delta\Phi$ of Σ^0 in Scenario I (bule dash-dot line) changes rapidly by 180° within 80 MeV above the threshold, whereas in Scenario II (orange dash-dot line) it varies more smoothly. After 2.7 GeV, both cases exhibit relatively stable phases. The corresponding polarization P_y of Σ^0 is shown in Fig. 2(b). Near the threshold, both cases possess the same polarization behavior but show completely opposite results after 2.45 GeV, and will present significant polarization effects at 2.5–2.6 GeV. On the other hand, from Fig. 2(b) (dotted line), it is evident that the peak polarization of Σ^- occurs near the $\phi(3D)$ and $\rho(2850)$ resonance states, with a variation pattern closely resembling the polarization evolution of Σ^+.

3.2. The $\Lambda \to \bar{\Sigma}^0$ Transition EMFFs. In the $e^+e^- \to \Lambda\bar{\Sigma}^0$ reaction, the total isospin of the Λ and $\bar{\Sigma}^0$ system is 1, which means that only vector particles with isospin 1 contribute to the process in the VMD model. Thus, the ρ and excited $\rho(3D)$ state are introduced, resulting in four parameters γ, $\beta_\rho^{\Lambda\bar{\Sigma}^0}$, $\beta_{\rho(3D)}^{\Lambda\bar{\Sigma}^0}$, and $\alpha_{\rho(3D)}^{\Lambda\bar{\Sigma}^0}$ that need to be determined. Firstly, we fixed γ at 0.43 for the intrinsic form factor $g(q^2)$. This form factor reflects the internal structure of the three valence quarks within the baryon.[81] According to the quark model, both Σ and Λ particles contain one strange quark and two light-flavor quarks with the same flavor structure.

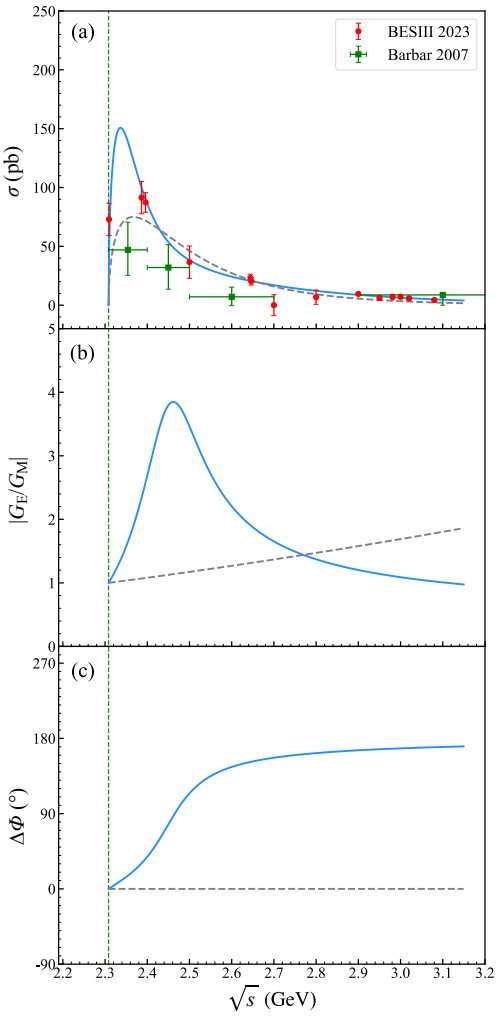

Fig. 6. The obtained total cross-sections of the process $e^+e^- \to \Lambda\bar{\Sigma}^0$ comparing with the experimental data, and the prediction for the ratio $|G_E/G_M|$ and relative phase $\Delta\Phi$. The blue solid line represents the inclusion of the $\rho(3D)$, while the dashed line is the exclusion of $\rho(3D)$. The experimental data are taken from Refs. [6,16].

Furthermore, previous studies on the $e^+e^- \to \Lambda\bar{\Lambda}$ reaction report a γ value of 0.43 GeV^{-2},[35] which aligns well with our work's γ value for Σ, ranging from 0.4217 to 0.4662 GeV^{-2}. Given these similarities, we assumed the γ parameter for the $e^+e^- \to \Lambda\bar{\Sigma}^0$ process were consistent with values from reactions $e^+e^- \to \Sigma\bar{\Sigma}$ and $e^+e^- \to \Lambda\bar{\Lambda}$, and hence fixed at 0.43 GeV^{-2}. Besides, in Refs. [82,83], it was found that the vector coupling constant of $g_{\Sigma\Lambda\rho}$ is 0. Since $\beta_\rho^{\Lambda\bar{\Sigma}^0}$ is proportional to $g_{\Sigma\Lambda\rho}$, we fixed the parameter $\beta_\rho^{\Lambda\bar{\Sigma}^0} = 0$. For the remaining parameters, we determined them by fitting to the total cross-section data from BESIII Collaboration,[16] excluding BaBar data due to large experimental uncertainties.[6] The resulting fitted parameters were $\beta_{\rho(3D)}^{\Lambda\bar{\Sigma}^0} = 0.3784$, $\alpha_{\rho(3D)}^{\Lambda\bar{\Sigma}^0} = -0.4053$, with χ^2/d.o.f achieving a value of 1.0.

In Fig. 6, we compare our fit to the experimental data. The blue solid line includes the contribution of $\rho(3D)$, while the gray dashed line represents a fit without $\rho(3D)$ (achieved by setting the $\beta_{\rho(3D)}$ and $\alpha_{\rho(3D)}$ coupling constant to zero). As shown in Fig. 6(a), we can see that

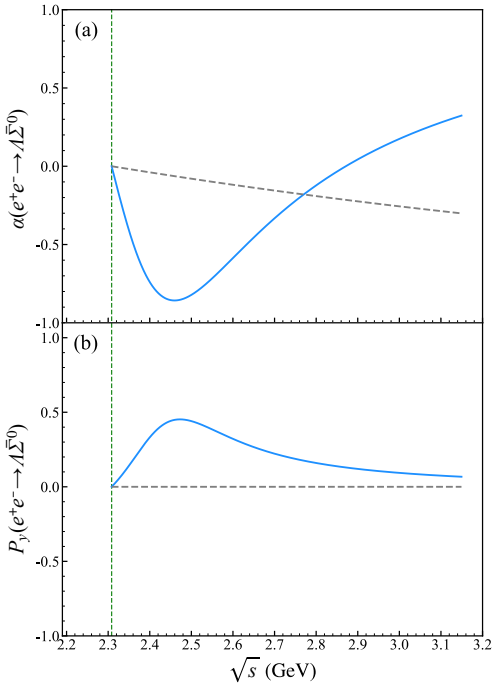

Fig. 7. The obtained angular distribution parameter α and polarization P_y of $\Lambda\bar{\Sigma}^0$. The blue solid line represents the inclusion of the $\rho(3D)$, while the dashed line is the exclusion of $\rho(3D)$.

the blue solid line and the gray dashed line provide a reasonable description of the total cross-section. However, the blue solid line shows a notable enhancement near the threshold, with cross-sections reaching approximately 150 pb. This increase is attributed to the influence of $\rho(3D)$ near the threshold, consistent with certain theoretical explanations for the threshold enhancement in the $e^+e^-\to\Lambda\bar{\Lambda}$ process.[31,35,84]

As a prediction, we also present the electromagnetic ratio $|G_{\rm E}/G_{\rm M}|$ and relative phase $\Delta\Phi$ for the Λ–$\bar{\Sigma}^0$ system, shown in Figs. 6(b) and 6(c), respectively. In Fig. 6(b), the blue solid line, which includes $\rho(3D)$, exhibits a distinct non-monotonic behavior compared to the gray dashed line without $\rho(3D)$. Starting near the threshold, the ratio $|G_{\rm E}/G_{\rm M}|$ first increases, then decreases, eventually stabilizing at 1 in the higher energy region. One can note that the ratio $|G_{\rm E}/G_{\rm M}|$ approaches a large value at a center-of-mass energy of $\sqrt{s}=2.46$ GeV, where the angular distribution parameter α converges to -1, as shown in Fig. 7(a). This indicates the possibility of observing a clear angular distribution for the final state in the reaction $e^+e^-\to\Lambda\bar{\Sigma}^0$ near this energy. Additionally, as shown in Fig. 6(c), the relative phase increases steadily from 0° to 180° as the center-of-mass energy rises, reaching 90° at 2.46 GeV and suggesting the possibility of significant polarization effects. Finally, in Fig. 7(b) we show the numerical results of the polarization P_y, exhibiting a pronounced peak within the energy range of 2.4 to 2.5 GeV.

4. Summary. In this work, we study the EMFFs of Σ and Λ–$\bar{\Sigma}^0$ transition form factors in the timelike region using a phenomenological extending VMD model. In the reaction $e^+e^-\to\Sigma\bar{\Sigma}$, in addition to ground mesons ρ, ω, and ϕ, we take account into additional vector meson excited states $\rho(3D)$, $\omega(3D)$, $\phi(3D)$, and $\rho(2850)$. We split into two scenarios according to the contribution of $\rho(3D)$ and $\omega(3D)$. With these vector mesons, both scenarios can successfully describe the total cross-section of the Σ isospin triplet state, as well as the electromagnetic ratio $|G_{\rm E}/G_{\rm M}|$ and relative phase $\Delta\Phi$ of Σ^+. Our results show a significant enhancement of the total cross-section around a center-of-mass energy of 2.5 GeV compared to only using ground state vector mesons, which is mainly due to the effect of $\phi(3D)$. This also gives a natural explanation for the cross-section recently measured by BESIII. Furthermore, we find that the electromagnetic ratio of Σ^+ exhibits a decreasing oscillatory behavior, a feature very similar to that in $\Lambda_{\rm c}^+$.

Our analysis for the process of $e^+e^-\to\Lambda\bar{\Sigma}^0$ finds that the $\rho(3D)$ state plays a crucial role in the threshold enhancement of the total cross-section. Notably, despite the $\rho(3D)$ lying below the reaction threshold, it significantly impacts the EMFFs above the threshold. This effect is particularly pronounced in the ratio $|G_{\rm E}/G_{\rm M}|$ and its associated $\Delta\Phi$ across a wide energy range.

Finally, we emphasize that in the $e^+e^-\to\Sigma\bar{\Sigma}$ and $\Lambda\bar{\Sigma}^0$ processes, the non-monotonic structures of the total cross-sections, the ratio $|G_{\rm E}/G_{\rm M}|$, and the non-zero relative phase $\Delta\Phi$ can be naturally explained by the VMD model. In particular, the contributions of vector meson resonance states above the reaction threshold are important.

Acknowledgments. We would like to thank Prof. Xiong-Fei Wang for fruitful discussions. This work was partly supported by the National Key R&D Program of China (Grant No. 2023YFA1606703), and the National Natural Science Foundation of China (Grant Nos. 12435007, 12361141819, 12275185, and 12335002).

References

[1] Denig A and Salme G 2013 *Prog. Part. Nucl. Phys.* **68** 113
[2] Pacetti S, Baldini Ferroli R, and Tomasi-Gustafsson E 2015 *Phys. Rept.* **550-551** 1
[3] Punjabi V, Perdrisat C F, Jones M K, Brash E J, and Carlson C E 2015 *Eur. Phys. J. A* **51** 79
[4] Mangoni A, Pacetti S, and Tomasi-Gustafsson E 2021 *Phys. Rev. D* **104** 116016
[5] Kuraev E A, Tomasi-Gustafsson E, and Dbeyssi A 2012 *Phys. Lett. B* **712** 240
[6] Aubert B, Bona M, Boutigny D *et al.* (BABAR Collaboration) 2007 *Phys. Rev. D* **76** 092006
[7] Ablikim M, Achasov M N, Ahmed S *et al.* (BESIII Collaboration) 2018 *Phys. Rev. D* **97** 032013
[8] Ablikim M, Achasov M N, Adlarson P *et al.* (BESIII Collaboration) 2010 *Phys. Rev. Lett.* **124** 032002
[9] Ablikim M, Achasov M N, Adlarson P *et al.* (BESIII Collaboration) 2019 *Phys. Rev. Lett.* **123** 122003
[10] Ablikim M, Achasov M N, Adlarson P *et al.* (BESIII Collaboration) 2021 *Phys. Lett. B* **820** 136557
[11] Ablikim M, Achasov M N, Adlarson P *et al.* (BESIII Collaboration) 2022 *Phys. Lett. B* **831** 137187
[12] Ablikim M, Achasov M N, Adlarson P *et al.* (BESIII Collaboration) 2021 *Phys. Rev. D* **104** L091104

[13] Gong G, Li L K, Zhang Y *et al.* (Belle Collaboration) 2023 *Phys. Rev. D* **107** 072008
[14] Ablikim M, Achasov M N, Adlarson P *et al.* (BESIII Collaboration) 2023 *JHEP* **2023** 228
[15] Ablikim M, Achasov M N, Adlarson P *et al.* (BESIII Collaboration) 2024 *Phys. Rev. D* **109** 034029
[16] Ablikim M, Achasov M N, Adlarson P *et al.* (BESIII Collaboration) 2024 *Phys. Rev. D* **109** 012002
[17] Ablikim M, Achasov M N, Adlarson P *et al.* (BESIII Collaboration) 2024 *JHEP* **2024** 022
[18] Huang G and Ferroli R B 2021 *Natl. Sci. Rev.* **8** nwab187
[19] Ablikim M, Achasov M N, Ahmed S *et al.* (BESIII Collaboration) 2019 *Nat. Phys.* **15** 613
[20] Ablikim M, Achasov M N, Adlarson P *et al.* (BESIII Collaboration) 2022 *Phys. Rev. D* **105** L011101
[21] Ablikim M, Achasov M N, Adlarson P *et al.* (BESIII Collaboration) 2022 *Phys. Rev. Lett.* **129** 131801
[22] Ablikim M, Achasov M N, Adlarson P *et al.* (BESIII Collaboration) 2023 *JHEP* **10** 81
[23] Ablikim M, Achasov M N, Adlarson P *et al.* (BESIII Collaboration) 2020 *Phys. Rev. Lett.* **125** 052004
[24] Ablikim M, Achasov M N, Adlarson P *et al.* (BESIII Collaboration) 2024 *Phys. Rev. Lett.* **132** 081904
[25] Ablikim M, Achasov M N, Adlarson P *et al.* (BESIII Collaboration) 2024 *Phys. Rev. Lett.* **133** 101902
[26] Ablikim M, Achasov M N, Adlarson P *et al.* (BESIII Collaboration) 2024 *JHEP* **2024** 186
[27] Ablikim M, Achasov M N, Adlarson P *et al.* (BESIII Collaboration) 2022 *Phys. Rev. D* **106** L091101
[28] Ablikim M, Achasov M N, Adlarson P *et al.* (BESIII Collaboration) 2023 *Phys. Rev. D* **108** L031106
[29] Ablikim M, Achasov M N, Adlarson P *et al.* (BESIII Collaboration) 2023 *Phys. Rev. D* **108** L011101
[30] Liu H, Zhang J, and Wang X 2023 *Symmetry* **15** 214
[31] Cao X, Dai J P, and Xie Y P 2018 *Phys. Rev. D* **98** 094006
[32] Yang Y, Chen D Y, and Lu Z 2019 *Phys. Rev. D* **100** 073007
[33] Haidenbauer J, Meißner U G, and Dai L Y 2021 *Phys. Rev. D* **103** 014028
[34] Li Z Y and Xie J J 2021 *Commun. Theor. Phys.* **73** 055201
[35] Li Z Y, Dai A X, and Xie J J 2022 *Chin. Phys. Lett.* **39** 011201
[36] Dai A X, Li Z Y, Chang L, and Xie J J 2022 *Chin. Phys. C* **46** 073104
[37] Yan B, Chen C, and Xie J J 2023 *Phys. Rev. D* **107** 076008
[38] Chen C, B. Yan B, and Xie J J 2025 *Chin. Phys. C* **49** 023102
[39] Lin Y H, Hammer H W, and Meißner U G 2022 *Eur. Phys. J. C* **82** 1091
[40] Dai J P, Cao X, and Lenske H 2023 *Phys. Lett. B* **846** 138192
[41] Lin Y H, Guo F K, and Meißner U G 2024 *Phys. Lett. B* **856** 138887
[42] Cao X, Liang Y T, and Ping R G 2024 *Phys. Rev. D* **110** 014035
[43] Zhang Z, Ping R G, Liu T, Song J J, Yang W, and Zhou Y J 2024 *Phys. Rev. D* **110** 034034
[44] Zheng W, Kupsc A, Pacetti S, Rosini F, Salone N, Wang X, and Fang S S 2025 *Chin. Phys. Lett.* **42** 041201
[45] Dai L Y, Haidenbauer J, and Meißner U G 2025 *Chin. Phys. Lett.* **42** 030202
[46] Ablikim M, Achasov M N, Adlarson P *et al.* (BESIII Collaboration) 2021 *Phys. Lett. B* **814** 136110
[47] Mangoni A 2022 *SciPost Phys. Proc.* **10** 021
[48] Irshad M, Liu D, Zhou X, and Huang G 2022 *Symmetry* **14** 69
[49] Ramalho G, Peña M T, and Tsushima K 2020 *Phys. Rev. D* **101** 014014
[50] Anselmino M, Predazzi E, Ekelin S, Fredriksson S, and Lichtenberg D B 1993 *Rev. Mod. Phys.* **65** 1199
[51] Kubis B and Meissner U G 2001 *Eur. Phys. J. C* **18** 747
[52] Iachello F, Jackson A D, and Lande A 1973 *Phys. Lett. B* **43** 191
[53] Iachello F and Wan Q 2004 *Phys. Rev. C* **69** 055204
[54] Bijker R and Iachello F 2004 *Phys. Rev. C* **69** 068201
[55] Yan B, Chen C, Li X, and Xie J J 2024 *Phys. Rev. D* **109** 036033
[56] Bisello D, Busetto G, Castro A *et al.* (DM2 Collaboration) 1990 *Z. Phys. C* **48** 23
[57] Haidenbauer J, Holinde K, and Speth J 1993 *Nucl. Phys. A* **562** 317
[58] Navas S, Amsler C, Gutsche T *et al.* (Particle Data Group Collaboration) 2024 *Phys. Rev. D* **110** 030001
[59] Pang C Q, Wang Y R, Hu J F, Zhang T J, and Liu X 2020 *Phys. Rev. D* **101** 074022
[60] Wang J Z, Wang L M, Liu X, and Matsuki T 2021 *Phys. Rev. D* **104** 054045
[61] Wang L M, Luo S Q, and Liu X 2022 *Phys. Rev. D* **105** 034011
[62] Feng J C, Kang X W, Lü Q F, and Zhang F S 2021 *Phys. Rev. D* **104** 054027
[63] Zhou Q S, Wang J Z, and Liu X 2022 *Phys. Rev. D* **106** 034010
[64] Zhou Q S, Wang J Z, Liu X, and Matsuki T 2022 *Phys. Rev. D* **105** 074035
[65] Wang Y R, Li T Y, Fang Z Y, Chen H, and Pang C Q 2022 *Phys. Rev. D* **106** 114024
[66] Wang Y R, Ma Y, and Pang C Q 2023 *Int. J. Mod. Phys. A* **38** 2350118
[67] Bai Z Y, Zhou Q S, and Liu X 2023 *Phys. Rev. D* **108** 094036
[68] Lodha C and Rai A K 2024 *Eur. Phys. J. Plus* **139** 663
[69] Lodha C and Rai A K 2024 *Few Body Syst.* **65** 99
[70] Feng X C, Li Z Y, Li D M, Song Q T, Wang E, and Yan W C 2022 *Phys. Rev. D* **106** 076012
[71] Sakharov A D 1948 *Zh. Eksp. Teor. Fiz.* **18** 631
[72] Fäldt G and Kupsc A 2017 *Phys. Lett. B* **772** 16
[73] Granados C, Leupold S, and Perotti E 2017 *Eur. Phys. J. A* **53** 117
[74] Lepage G P and Brodsky S J 1979 *Phys. Rev. Lett.* **43** 545
[75] Lepage G P and Brodsky S J 1980 *Phys. Rev. D* **22** 2157
[76] Belitsky A V, Ji X D, and Yuan F 2003 *Phys. Rev. Lett.* **91** 092003
[77] Leinweber D B, Woloshyn R M, and Draper T 1991 *Phys. Rev. D* **43** 1659
[78] Aliev T M, Ozpineci A, and Savci M 2001 *Phys. Lett. B* **516** 299
[79] Ablikim M, Achasov M N, Adlarson P *et al.* (BESIII Collaboration) 2023 *Phys. Rev. Lett.* **131** 191901
[80] Chen C, Yan B, and Xie J J 2024 *Chin. Phys. Lett.* **41** 021302
[81] Bijker R, Iachello F, and Leviatan A 1996 *Phys. Rev. C* **54** 1935
[82] Lai C S 1967 *Phys. Rev.* **155** 1562
[83] Erkol G, Timmermans R G E, and Rijken T A 2006 *Phys. Rev. C* **74** 045201
[84] Xiao L Y, Weng X Z, Zhong X H, and Zhu S L 2019 *Chin. Phys. C* **43** 113105